Journal of Sound and Vibration (1997) **206**(1), 15–22

DETERMINATION OF THE ASYNCHRONOUS LOAD ON A ROTOR FROM THE MEASURED INTERNAL FORCES

A.-V. PHAN AND G. REYNAUD

Institut National Polytechnique de Grenoble (*INPG*), *ENSHMG* (*CREMHyG*), *BP* 95, 38402 *St-Martin-d'Hères cedex*, *France*

(*Received* 16 *February* 1995, *and in final form* 24 *February* 1997)

Experimental contributions currently play an important role in determining hydraulic forces due to cavitation. Up to the present date, there is no computational analysis which has proven to be successful in this domain. Experiments are usually carried out to measure the resulting internal forces in a model because these forces are crucial for designing elements under cavitational flows. This paper presents a numerical approach using the theory of rotordynamics coupled with the finite element method (FEM) to determine the hydraulic load on a rotor from the internal forces measured in a cross-section of the rotor. Once the load is found, a program developed can be used to compute the internal forces in any cross-section of interest and to evaluate dynamic effects on the rotor. Two illustrative examples are presented to show the validity of this approach.

1. INTRODUCTION

A model of a future hydrogen pump has been developed at the Société Européenne de Propulsion (SEP). This is a multi-stage pump whose first stage, called the inducer, is an axial compressor which plays a prominent part in the overall efficiency of the engine in which the pump is installed. The inducer has been designed to endure cavitational flows.

In the scope of the research on this pump, the SEP has entrusted the Centre de Recherches et d'Essais de Machines Hydrauliques de Grenoble (CREMHyG) with the investigation of non-stationary forces generated by the cavitational fluid on the inducer. The current theories are inadequate to describe properly these time-dependent hydraulic loads, especially when the flow rate changes. Therefore, measurements of the forces on a model give the most reliable results [1, 2].

Experiments have been carried out at CREMHyG to measure the six components of internal forces (see Figure 1) in a cross-section of the pump rotor (see Figure 2). These internal forces are axial force (N_y), shear forces (T_x, T_z), torque (M_y) and bending moments (M_x, M_z). The measurements as well as the spectral analyses of the measured outputs were addressed in references [3] and [4].

This paper presents an FEM dynamic formulation and its numerical implementation for determining the asynchronous hydraulic load on the inducer from the internal forces measured in a cross-section of the rotor. To this end, first of all, a mathematical relationship between these two kinds of forces needs to be derived. Then, the load determination follows from an identification between experimental data and computed solutions.

0022–460X/97/360015 + 08 $25.00/0/sv971080

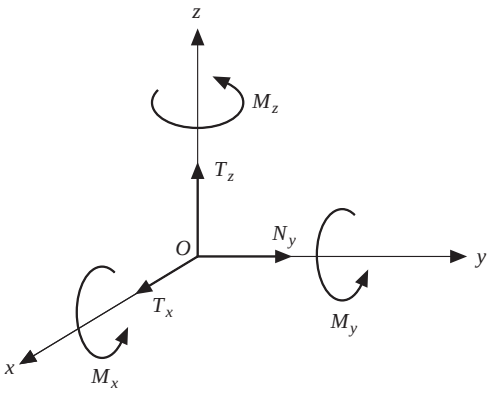

Figure 1. Internal forces (xz: cross-section plane, y: rotor axis).

Numerical results are presented for two illustrative examples. Finally, based on the developed mathematical relationship between internal and external forces, the effects of dynamic factors on the rotor behaviour are studied.

2. ANALYSIS OF TIME-DEPENDENT INTERNAL FORCES IN A ROTOR

2.1. FINITE ELEMENT FORMULATION OF THE SHEAR FORCES AND BENDING MOMENTS

Consider a rotor turning with an angular velocity ω and subjected to an asynchronous rotating force $\{F\}$ of angular velocity $\Omega = 2\pi f$, where f is the force frequency. The focus here is on the shear forces and bending moments since the experiments performed have shown that N_y and M_y are mostly static. In this case the external force under consideration should be a radial force. Let G be its intersection point with the rotor axis. The rotor is modelled by using $(N-1)$ shaft-beam finite elements. The global co-ordinate system XYZ is centered at G and each finite element is associated with a local Cartesian co-ordinate system xyz where Y and y coincide with the rotor axis as shown in Figure 3.

The nodal displacement component vectors of an element (i) can be written in its local co-ordinate system as follows

$$\{\delta_u(t)\} = \langle u_i(t), \psi_i(t), u_{i+1}(t), \psi_{i+1}(t)\rangle^{\mathrm{T}}, \qquad \{\delta_w(t)\} = \langle w_i(t), \theta_i(t), w_{i+1}(t), \theta_{i+1}(t)\rangle^{\mathrm{T}}, \quad (1)$$

where t is time, u_i, w_i, u_{i+1}, w_{i+1} are deflections in the x and z directions at nodes (i) and $(i+1)$, respectively, and ψ_i, θ_i, ψ_{i+1}, θ_{i+1} are slopes about the x and z directions at nodes (i) and $(i+1)$, respectively.

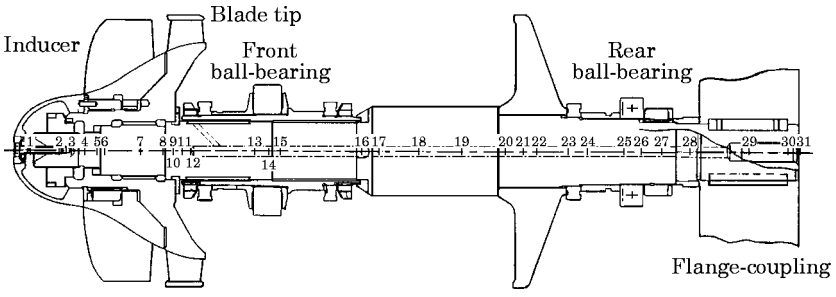

Figure 2. Rotor and its finite element mesh.

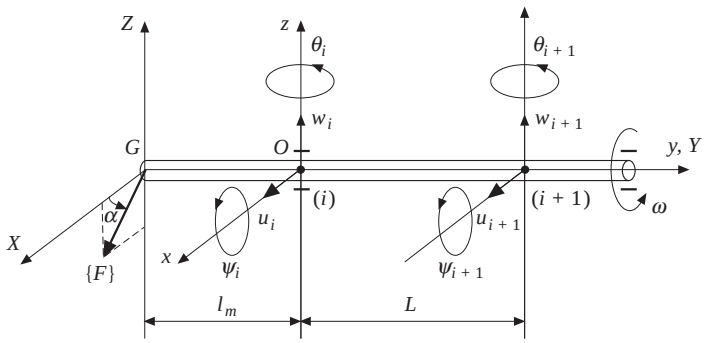

Figure 3. Global and local axes.

The familiar displacement shape functions for shaft-beam elements are

$$u(y, t) = a_1 + a_2 y + a_3 y^2 + a_4 y^3, \qquad w(y, t) = a_5 + a_6 y + a_7 y^2 + a_8 y^3, \tag{2}$$

in which the unknown coefficients $a_1, \ldots, a_8$ can be described in terms of the nodal displacements (1) by solving the following boundary condition equations (L is the length of element (i)):

$$u(0, t) = u_i(t), \qquad w(0, t) = w_i(t), \qquad u(L, t) = u_{i+1}(t), \qquad w(L, t) = w_{i+1}(t),$$
$$\psi(0, t) = \partial u/\partial y|_{y=0} = \psi_i(t), \qquad \theta(0, t) = \partial w/\partial y|_{y=0} = \theta_i(t),$$
$$\psi(L, t) = \partial u/\partial y|_{y=L} = \psi_{i+1}(t), \qquad \theta(L, t) = \partial w/\partial y|_{y=L} = \theta_{i+1}(t). \tag{3}$$

Thus equations (2) can now be rewritten in matrix form as

$$u(y, t) = \{N_1(y)\}^{\mathrm{T}}\{\delta_u(t)\}, \qquad w(y, t) = \{N_2(y)\}^{\mathrm{T}}\{\delta_w(t)\}, \tag{4}$$

where the shape vectors $\{N_1(y)\}$ and $\{N_2(y)\}$ are

$$\{N_1(y)\} = \left\langle 1 - \frac{3y^2}{L^2} + \frac{2y^3}{L^3}, -y + \frac{2y^2}{L} - \frac{y^3}{L^2}, \frac{3y^2}{L^2} - \frac{2y^3}{L^3}, \frac{y^2}{L} - \frac{y^3}{L^2} \right\rangle^{\mathrm{T}},$$

$$\{N_2(y)\} = \left\langle 1 - \frac{3y^2}{L^2} + \frac{2y^3}{L^3}, y - \frac{2y^2}{L} + \frac{y^3}{L^2}, \frac{3y^2}{L^2} - \frac{2y^3}{L^3}, -\frac{y^2}{L} + \frac{y^3}{L^2} \right\rangle^{\mathrm{T}} \tag{5}$$

It should be recalled that there are two theories for modelling of a beam at rest ($\omega = 0$) (see references [5] or [6], for example): Timoshenko beam theory includes rotatory inertia about the x- and z-axes (Rayleigh effect) and shear effect, whereas Bernoulli–Euler beam theory does not take these effects into account. Furthermore, since rotors are rotating beams, these two theories can also be employed for rotor modelling provided that the rotatory inertia about rotor axis (Y-axis) and the gyroscopic (Coriolis) effect are included in the models. The Timoshenko model is general and thus it is appropriate in most engineering problems. However this theory requires complex computations.

For a long beam where the beam diameter is much smaller than its length, it is valid to ignore the shear and Rayleigh effects. The present work considers the rotor under consideration (shown in Figure 2) as a long beam, so Bernoulli–Euler beam theory is employed here.

In this case, the bending moments and shear forces in element (i) are written as (see reference [7] for example)

$$M_x(y,t) = EI\,\partial^2 w/\partial y^2 = EI\{N_2''(y)\}^{\mathrm{T}}\{\delta_w(t)\},$$
$$M_z(y,t) = -EI\,\partial^2 u/\partial y^2 = -EI\{N_1''(y)\}^{\mathrm{T}}\{\delta_u(t)\}, \tag{6}$$
$$T_z(y,t) = -EI\,\partial^3 w/\partial y^3 = -EI\{N_2'''(y)\}^{\mathrm{T}}\{\delta_w(t)\},$$
$$T_x(y,t) = EI\,\partial^3 u/\partial y^3 = EI\{N_1'''(y)\}^{\mathrm{T}}\{\delta_u(t)\}, \tag{7}$$

where E and I are the Young's modulus of the material and cross-sectional moment of inertia, respectively. In equations (6) and (7) the rotatory inertia about the rotor axis and the gyroscopic effect are included by using the appropriate nodal displacement vectors $\{\delta_u(t)\}$ and $\{\delta_w(t)\}$. This is shown in detail in section 2.2.

The internal forces of interest are at node (i) since this node is associated with the cross-section where the measurements are taken. The expressions for the bending moments and shear forces at node (i) where $y = 0$ can be derived easily from equations (6) and (7) to yield

$$M_{xi}(t) = M_x(0,t) = EI\{N_2''(0)\}^{\mathrm{T}}\{\delta_w(t)\}, \qquad M_{zi}(t) = M_z(0,t) = -EI\{N_1''(0)\}^{\mathrm{T}}\{\delta_u(t)\},$$
$$T_{zi}(t) = T_z(0,t) = -EI\{N_2'''(0)\}^{\mathrm{T}}\{\delta_w(t)\}, \qquad T_{xi}(t) = T_x(0,t) = EI\{N_1'''(0)\}^{\mathrm{T}}\{\delta_u(t)\}. \tag{8}$$

The components in equations (8) are generated by the action of the asynchronous force $\{F\}$. Thus, in order to obtain these terms, the vectors $\{\delta_u(t)\}$ and $\{\delta_w(t)\}$ need to be determined from the corresponding dynamic equations of the rotor.

2.2. SOLUTION

It is assumed that at $t = 0$ the asynchronous load $\{F\}$ is an angle α with respect to the X-axis. The load components in X and Z directions are

$$\begin{Bmatrix} F_X \\ F_Z \end{Bmatrix} = \begin{Bmatrix} F_a\cos(\Omega t + \alpha) \\ -F_a\sin(\Omega t + \alpha) \end{Bmatrix} = \begin{Bmatrix} F_c \\ -F_s \end{Bmatrix}\cos(\Omega t) + \begin{Bmatrix} -F_s \\ -F_c \end{Bmatrix}\sin(\Omega t), \tag{9}$$

in which, F_a is the amplitude of the load, $F_c = F_a\cos\alpha$ and $F_s = F_a\sin\alpha$.

A simpler form of equation (9) is

$$\{F\} = \{F_1\}\cos(\Omega t) + \{F_2\}\sin(\Omega t). \tag{10}$$

By denoting $\{\bar{F}_1\}$ and $\{\bar{F}_2\}$ as the extensions of $\{F_1\}$ and $\{F_2\}$ over the whole structure, and letting

$$\{\delta\} = \langle u_1(t), w_1(t), \theta_1(t), \psi_1(t), \ldots, u_N(t), w_N(t), \theta_N(t), \psi_N(t)\rangle^{\mathrm{T}}, \tag{11}$$

then the differential equations of rotor motion are given in matrix form by [8]

$$([M] + [M_s])\{\ddot{\delta}\} + ([A] + \omega[C])\{\dot{\delta}\} + [K]\{\delta\} = \{\bar{F}_1\}\cos(\Omega t) + \{\bar{F}_2\}\sin(\Omega t). \tag{12}$$

In equation (12), $[M]$, $[M_s]$, $[A]$, $[C]$, $[K]$ are, respectively, classical mass, secondary mass, damping, Coriolis and stiffness matrices (global matrices) which are found by assembling the corresponding element matrices of all the structural components of the rotor. It should be noted that $[\mathrm{M_s}]$ and $[C]$ give, respectively, the influence of the secondary effect of rotatory inertia about rotor axis and the gyroscopic effect [8].

Here, the system (12) is solved by using the code ROTOR developed at Laboratoire de Mécanique des Structures (INSA de Lyon), and the response $\{\delta\}$ is obtained in the form

$$\{\delta\} = \{\Delta_1\}\cos(\Omega t) + \{\Delta_2\}\sin(\Omega t) \tag{13}$$

where

$$\{\Delta_1\} = \langle \Delta_{1u1}, \Delta_{1w1}, \Delta_{1\theta1}, \Delta_{1\psi1}, \ldots, \Delta_{1uN}, \Delta_{1wN}, \Delta_{1\theta N}, \Delta_{1\psi N}\rangle^{\mathrm{T}},$$
$$\{\Delta_2\} = \langle \Delta_{2u1}, \Delta_{2w1}, \Delta_{2\theta1}, \Delta_{2\psi1}, \ldots, \Delta_{2uN}, \Delta_{2wN}, \Delta_{2\theta N}, \Delta_{2\psi N}\rangle^{\mathrm{T}}. \tag{14}$$

This response $\{\delta\}$ takes the effect of rotatory inertia about rotor axis and the gyroscopic effect into account as mentioned above since the terms $[M_s]$ and $\omega[C]$ are included in equation (12).

Substituting $\{\delta_u(t)\}$ and $\{\delta_w(t)\}$ derived from equations (14) into equations (8) yields

$$M_{ki}(t) = M_{ki1}\cos(\Omega t) + M_{ki2}\sin(\Omega t) = \bar{M}_{ki}\cos(\Omega t + \beta_{Mk}),$$
$$T_{ki}(t) = T_{ki1}\cos(\Omega t) + T_{ki2}\sin(\Omega t) = \bar{T}_{ki}\cos(\Omega t + \beta_{Tk}), \tag{15}$$

in which,

$$\bar{M}_{ki} = \sqrt{M_{ki1}^2 + M_{ki2}^2}, \qquad \bar{T}_{ki} = \sqrt{T_{ki1}^2 + T_{ki2}^2},$$
$$\tan(\beta_{Mk}) = -M_{ki2}/M_{ki1}, \qquad \tan(\beta_{Tk}) = -T_{ki2}/T_{ki1}, \qquad k \equiv x, z, \tag{16}$$

and,

$$M_{xij} = (2EI/L)(-(3/L)\Delta_{jw1} - 2\Delta_{j\theta1} + (3/L)\Delta_{jw2} - \Delta_{j\theta2}),$$
$$M_{zij} = (2EI/L)((3/L)\Delta_{ju1} - 2\Delta_{j\psi1} - (3/L)\Delta_{ju2} - \Delta_{j\psi2}),$$
$$T_{zij} = (6EI/L^2)(-(2/L)\Delta_{jw1} - \Delta_{j\theta1} + (2/L)\Delta_{jw2} - \Delta_{j\theta2}),$$
$$T_{xij} = (6EI/L^2)((2/L)\Delta_{ju1} - \Delta_{j\psi1} - (2/L)\Delta_{ju2} - \Delta_{j\psi2}), \qquad j = 1, 2. \tag{17}$$

It can be seen from equations (15) that the resulting bending moments and shear forces have the same Ω (i.e., the same frequency f) as the asynchronous load $\{F\}$.

3. DETERMINATION OF THE HYDRAULIC LOAD

3.1. SPECTRAL ANALYSIS OF EXPERIMENTAL RESULTS

Consider an experiment which is carried out by decreasing the suction pressure p at a fixed angular velocity of the rotor ($\omega = 7500$ r.p.m.) and at a nominal flow rate. In this case, when the pressure is lower than a certain threshold, cavitational flow is generated and the measurement of the internal forces is taken. Spectral analysis is then employed to evaluate the variation of these measured forces which can now be described as

$$Q(t) = \frac{Q_0}{2} + \sum_{n=1}^{\infty} Q_n \cos(2\pi f_n t + \varphi_n), \tag{18}$$

where $Q(t)$ denotes the measured internal forces, Q_0 is amplitude of the static component, and Q_n, f_n and φ_n are, respectively, amplitude, frequency and phase of nth time-dependent component.

Q_0, Q_n and f_n can be determined from response spectra of these measured signals. For example, Figure 4 shows response spectra of the bending moment M_x measured from the

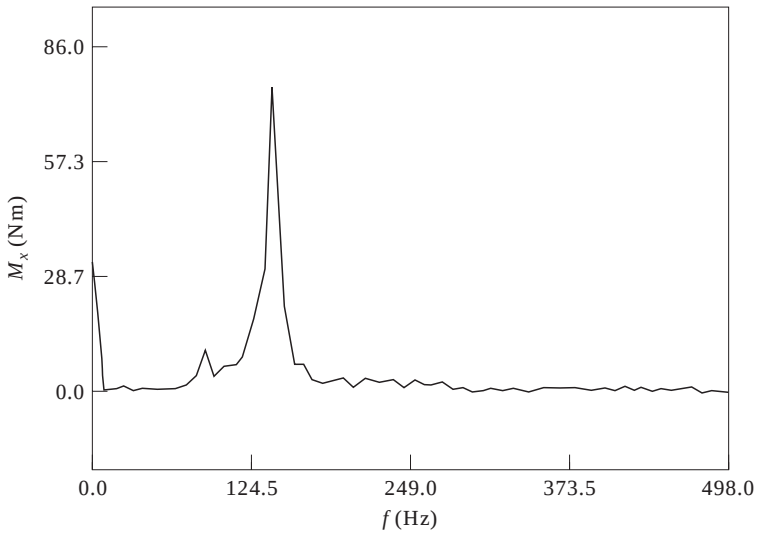

Figure 4. Response spectra of the bending moment M_x.

above experiment. Since only three important spectra are observed from this figure, equation (18) in this case can be written as

$$M_x(t) \approx \frac{M_{x0}}{2} + \sum_{n=1}^{2} M_{xn} \cos(2\pi f_n t + \varphi_{Mn}). \tag{19}$$

Numerical analyses are performed for all six internal forces. The results given in Tables 1 and 2 are two examples which correspond to two different suction pressures.

3.2. IDENTIFICATION

An identification between the numerical analysis and the experimental results needs to be done to determine the hydraulic load from the measured internal forces. It can be seen that there is no problem identifying the load components corresponding to N_y and M_y which are time-independent as shown in Tables 1 and 2. So the task is how to determine

TABLE 1

Spectral analysis results for pressure $p = 0{\cdot}961$ bar

n	f_n (Hz)	M_{yn} (Nm)	N_{yn} (N)	M_{xn} (Nm)	M_{zn} (Nm)	T_{xn} (N)	T_{zn} (N)
0	0	656	47625	−27·3	8·2	67·3	−57·5
1	86	0·0	0·0	10·8	12·2	198·1	180·4
2	141	0·0	0·0	76·5	72·6	1456·6	1462·5

TABLE 2

Spectral analysis results for pressure $p = 0{\cdot}655$ bar

n	f_n (Hz)	M_{yn} (Nm)	N_{yn} (N)	M_{xn} (Nm)	M_{zn} (Nm)	T_{xn} (N)	T_{zn} (N)
0	0	654	47475	20·0	23·5	−65·1	24·3
1	125	0·0	0·0	76·4	75·4	2005·2	2041·5
2	250	0·0	0·0	3·2	4·4	55·5	50·6

TABLE 3

Computed results for pressure $p = 0{\cdot}961$ bar

n	f_n (Hz)	Δl_n (mm)	F_n (N)	$\bar{M}_{xn}$ (Nm)	$\bar{M}_{zn}$ (Nm)	$\bar{T}_{xn}$ (N)	$\bar{T}_{zn}$ (N)
1	86	0·1	170	8·8	9·2	201·1	191·0
2	141	1·2	1000	64·4	78·4	1736·3	1472·8

the radial load which results in the time-dependent internal forces M_x, M_z, T_x and T_z presented in these tables.

As discussed before, the internal forces have the same frequency f as the external load. It follows that each time-dependent set (M_{xn}, M_{zn}, T_{xn}, T_{zn}) of frequency $f_n > 0$ Hz (see Tables 1 and 2) can be associated with a load component of the same f_n and is determined by using equations (15). The key is to choose, for each f_n, an amplitude F_n (used in equations (9)) of the load component and its application point so that the computed set ($\bar{M}_{xin}$, $\bar{M}_{zin}$, $\bar{T}_{xin}$, $\bar{T}_{zin}$) given by (15) and the measured set (M_{xn}, M_{zn}, T_{xn}, T_{zn}) are matched as closely as possible.

To this end, two subroutines used with the code ROTOR have been developed [9] in order to compute the internal forces (15) from a given asynchronous load.

Finally, an approximation expression for the hydraulic radial load can be written as

$$F_X(t) \approx \frac{T_{x0}}{2} + \sum_{n=1}^{2} F_n \cos(2\pi f_n t + \alpha_n), \qquad F_Z(t) \approx \frac{T_{z0}}{2} + \sum_{n=1}^{2} F_n \sin(2\pi f_n t + \alpha_n). \quad (20)$$

The computed numerical results are reported in Tables 3 and 4, in which Δl_n is the eccentricity between the center of gravity of the inducer blades (see Figure 2) and the application point of the load component found at the frequency f_n.

The determined load components of amplitude F_n result in the computed internal forces ($\bar{M}_{xin}$, $\bar{M}_{zin}$, $\bar{T}_{xin}$, $\bar{T}_{zin}$) shown in Tables 3 and 4. It is quite remarkable that these results are in good agreement with those measured (Tables 1 and 2).

4. EFFECTS OF DYNAMIC FACTORS ON THE INTERNAL FORCES

It can be seen that the success of the approach presented in this work depends on the accuracies of rotor modelling and the measured internal forces. The identification in section 3.2 can thus be used as a reference to verify these accuracies. Once a well matched identification is found, the rotor model can then be employed to evaluate effects of dynamic factors such as ω and Ω on the resulting amplitude of the time-dependent internal forces.

As an example, an asynchronous load of form (9) has been studied. Figure 5 shows the effects of ω and Ω on the ratios T_z/F_a and M_x/M_a where $M_a = F_a l_m$ and $F_a = 1000$ N. The fact that both T_z/F_a and M_x/M_a increase with the growth of Ω is not surprising. However, it can be noted that ω has almost no influence on the shear force whereas its effect is more important on the bending moment. The last point may be explained by the "stiffening" effect due to the gyroscopic effect provoked by the "flywheels".

TABLE 4

Computed results for pressure $p = 0{\cdot}655$ bar

n	f_n (Hz)	Δl_n (mm)	F_n (N)	$\bar{M}_{xn}$ (Nm)	$\bar{M}_{zn}$ (Nm)	$\bar{T}_{xn}$ (N)	$\bar{T}_{zn}$ (N)
1	125	8·2	1400	71·9	81·8	2124·2	1865·8
2	250	20·0	30	4·7	1·9	43·0	82·1

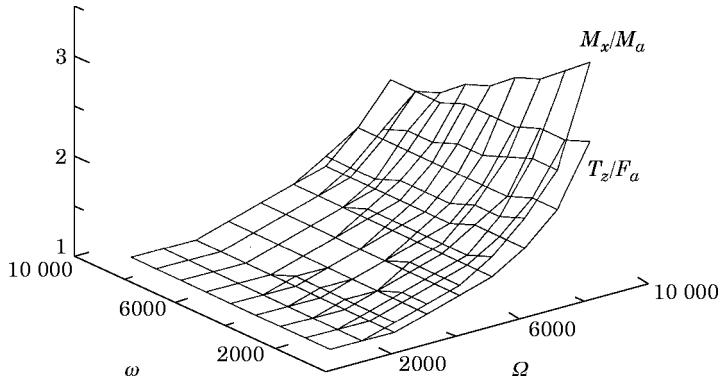

Figure 5. Dynamic effects of ω (r.p.m.) and Ω (r.p.m.) on $T_z(\omega, \Omega)/F_a$ and $M_x(\omega, \Omega)/M_a$.

5. CONCLUSIONS

A numerical analysis based on FEM rotor dynamics has been developed to determine a relationship between an asynchronous load on a rotor and its resulting internal forces. Once the internal forces in a given cross-section of the rotor are measured, this analysis enables the identification of the external load which can then be used to compute the internal forces at any desired cross-section. Also, the analysis can be employed to evaluate effects of dynamic factors on the time-dependent internal forces.

Finally this work certainly warrants further research to develop a more general analysis in which the shear and Rayleigh effects are taken into consideration.

ACKNOWLEDGMENTS

The authors wish to thank the SEP for making the content of this paper possible. They also express their appreciation for the helpful suggestions from G. Ferraris (Laboratoire de Mécanique des Structures, INSA de Lyon).

REFERENCES

1. P. Bachmann 1980 *Bulletin Escher Wyss*, 1/2 **53**, 69–81. Progrès dans la mesure des forces et couples sur les rotors des modèles de turbo-machines hydrauliques.
2. B. Hillary and D. J. Ewins 1984 *Second International Modal Analysis Conference*, *Orlando FL*, 627–634. The use of strain gage in force determination and frequency response function measurements.
3. C. Brunet 1991 *Masters Thesis*, *Ecole Nationale Supérieure d'Hydraulique et de Mécanique de Grenoble*, *Institut Polytechnique de Grenoble*, *France*. Etude expérimentale des efforts sur l'inducteur d'une turbo-pompe. Analyse dynamique de la ligne d'arbre.
4. G. Reynaud, C. Rebattet and C. Brunet 1993 *Fluids Engineering Conference*, *Washington DC*. Experimental and numerical investigations of the forces in a pump inducer.
5. R. W. Clough and J. Penzien 1993 *Dynamics of Structures*. New York: McGraw-Hill.
6. R. R. Craig 1981 *Structural Dynamics*. (*An Introduction to Computer Methods*). New York: John Wiley and Sons.
7. P. Trompette 1992 *Mécanique des Structures par la Méthode des Eléments Finis*. Paris: Masson.
8. M. Lalanne and G. Ferraris 1990 *Rotordynamics*. *Prediction in Engineering*. Chichester: John Wiley and Sons.
9. A.-V. Phan 1993 *Masters thesis*, *Ecole Nationale Supérieure d'Hydraulique et de Mécanique de Grenoble*, *Institut Polytechnique de Grenoble*, *France*. Bruits mécaniques dans la ligne d'arbre de la turbo-pompe du moteur Vulcain d'Ariane V.